

A MODEL FOR TRANSITION BETWEEN OUTDOOR AND INDOOR PROPAGATION

J. Blas, P. Fernández, R. M. Lorenzo, and E. J. Abril

Department of Signal Theory, Communications
and Telematics Engineering
University of Valladolid
Campus Miguel Delibes, Camino del Cementerio s/n 47011
Valladolid, Spain

S. Mazuelas, A. Bahillo, and D. Bullido

Center for the Development of Telecommunications of Castilla y León
CEDETEL, Edificio Solar, Parque Tecnológico de Boecillo 47151
Boecillo (Valladolid), Spain

Abstract—We present a novel outdoor-indoor radio wave propagation model. It predicts the electric field envelope Cumulative Distribution Function (CDF) in a room placed near a radio communication emitter. The experimental CDF obtained from the simulation, fits the experimental CDF obtained from a measurement campaign carried out over 19200 sampling points inside the room. The maximum deviation found between these CDFs is less than 1%. Kolmogorov-Smirnov test is employed to analyze the goodness of fit. P-values around 99% are reached. A comparison is made with other classical methods reported in the literature as ray-tracing (RT) and a hybrid method employing finite-difference time-domain (FDTD) together with RT. The proposed model significantly improves the results achieved in those previous investigations. Although we study the problem in three dimensions, the repetitive nature of the algorithm allows us to parallelize the computation process speeding the calculations.

1. INTRODUCTION

Site specific propagation models based on ray-tracing [1] are successfully employed to solve problems that meet simulation volumes and objects which are relatively large in comparison to wavelength.

This restriction is related to geometrical optics (GO) assumption of locally plane waves that impinge on surfaces with a curvature radius large enough to collect phase and amplitude information into rays avoiding a full wave approach. This model has been proven to be valid for both indoor [2–4] and outdoor propagation environments [5]. However, the transition between outdoor and indoor propagation is a problem that remains unsatisfactorily solved. The key issue is propagation through windows, which measure only a few wavelengths and present complex diffraction patterns, not easily described through a pure ray-tracing model [6]. In fact, although these models are usually supplemented by means of the uniform theory of diffraction (UTD), this theory is only rigorous for wedges of perfect electric conductors and as stated before, GO is restricted to electrically large objects [7–9].

In order to assess propagation through windows, asymptotic methods of low frequency, such as finite-difference time-domain (FDTD), are more appropriate than GO and UTD. This numerical technique incorporates constitutive relationships to describe in detail the response of the medium. Specifically, simulation volume is divided into electrically small cells, typically with a maximum size of 0.1λ . Each node of this sampling mesh has its own permittivity, conductivity and permeability, allowing a detailed representation of complex lossy structures and heterogeneous materials in detail [10, 11]. Some examples of indoor propagation models based on FDTD are [12–14]. In contrast to ray-tracing, this technique provides an exhaustive solution for simulation volumes that are relatively small in terms of wavelength [15, 16]. For large distances between radiating sources and scattering objects the dispersion propagated error is augmented. In addition, the small spatial sampling size (0.1λ) together with a large three dimensional scenario lead to an increase in the memory and time requirements until they become prohibitive. Some approaches resolve in part these problems. For instance, they reduce time and memory requirements of FDTD method in subsequent executions. After FDTD algorithm is executed one time, a transfer function [17] or an equivalent ray model [18] are obtained to avoid a new FDTD simulation. However, the computational volume must contain a room, which is electrically large, in the first simulation. As a result, the excitation source has to be placed close to the window and therefore this restricts the window illumination model. Consequently, a pure FDTD solution is not achievable without a massive computer system, nor is it completely suitable to solve the outdoor/indoor propagation problem.

A logical conclusion is that a hybrid technique based on combining ray-tracing and FDTD methods could take advantage of both

approaches, as rays can efficiently solve the problem of propagation through large empty volumes, and FDTD is able to cope with complex transition zones where a greater level of detail is needed [6, 18–22]. However, in general, hybrid models have an additional inherent complexity associated with the implementation of a separate interface between different simulation domains assigned to distinct numerical methods. This is specially true in the FDTD/ray-tracing model because one of the two methods works in the time domain and the other one in the frequency domain. It should be noted that an indoor environment would produce multiple reflections that, in turn, would cause bidirectional propagation in the FDTD domain bounding surface. Prediction of attenuation for systems with outdoor transmitting antennas and indoor users based on combining semi-empirical methods and ray-tracing [23] have also been proposed.

A key underlying issue, not usually addressed in the literature, is the level of detail necessary for the method to provide accurate results. However this is one of the biggest problems when it comes to applying the propagation model to a real situation. In fact the data collection needed to initialize the model represents one of the greatest costs. This is likely one of the reasons why many mobile phone operators do not use ray-tracing models to deploy base stations. So it is especially important to extract accurate information with the minimal detail of the objects that lie in the simulation volume. Accordingly, the proposed method is centered on the part of the problem which is easiest to describe with least amount of data: the empty space. In particular the empty space associated with windows, just covered by the window panes.

The similarity between a window and an aperture is not a new concept, it was mentioned, for example, in [6]. In that paper, the FDTD method is employed to assess an equivalent ray model as a substitute for the window in a pure ray-tracing model. In addition, it is stated that the window radiation pattern obtained by using FDTD was similar to that obtained from an aperture with uniform illumination. As such, the proposed hypothesis is backed up with previous work. Also note that [6] tries to avoid the direct integration of FDTD and ray-tracing which, as stated before, is not simple in a multi-reflection environment. With a bidimensional approximation, they needed 91 rays to mimic the FDTD solution along an observation line parallel to the window (4λ width, infinite height) and placed at least 10λ away in the absence of walls.

In our model, we will not take into account many details such as pillars, windowsills and so on, since it is not necessary for us to achieve a perfect match between measurements and predicted values for each point inside the room. Our aim is to correctly predict the

statistical distribution of the electric field components in a plane area over the floor. This is enough to provide bit error rate estimations and many other characteristics of the communications channel [24, 25]. From the point of view of human exposure assessment, this statistical distribution could also be a straightforward way to characterize the type of exposure [26].

2. WINDOW APERTURE MODEL

2.1. Sub-apertures: Shape and Number

An aperture with uniform illumination has a well-known far-field radiation pattern. However, if we consider the whole window as a single aperture, the far field model cannot be applied in the proximity of the window, leaving a big part of the room out of the analysis. Furthermore, this model would not correctly predict the diffraction caused by the window being illuminated by the incident field penetrating into the room from the exterior. To resolve this issue we treat the window as a collection of sub-apertures, each one satisfying the conventional far-field criteria. The use of sub-apertures to resolve aperture problems is not new, the *NEC* (*Numerical Electromagnetic Code*) has exploited this possibility with parabolic surface antennas. Accordingly, [27] describes a method to approximate a non-uniform aperture illumination by means of a set of overlapping sub-apertures with triangular distribution. In our case, each sub-aperture will have uniform illumination and there will not be any overlap between them.

Before establishing how many sub-apertures should be implemented we must decide their shape. A rectangular shape seems appropriate, as a set of rectangular sub-apertures fits perfectly into a rectangular window. The aspect ratio of the sub-apertures is also important. If we think of a single sub-aperture as an isolated radiator, the best alternative would be to choose a square shape to minimize the maximum phase error in the vertical and horizontal planes. However, it also seems reasonable to consider the window as a whole, taking into account its aspect ratio by keeping the same proportions for each sub-aperture. In fact, we could analyze the meaning of this assumption through the application of the sampling theorem to the window illumination in the vertical and horizontal axes. In particular, we assume a uniform distribution inside the aperture limits and therefore a 2-D separable Fourier transform. The Fourier transform of the two rectangle functions are expressed in terms of the sinc() function:

$$\text{sinc}(x) = \frac{\sin(x)}{x} \quad (1)$$

Consequently, after sampling one of this rectangle functions we will get an overlapping periodic sinc() function in the frequency domain due to aliasing. This overlap is more severe as the number of samples decreases. If we employ sub-apertures with an aspect ratio equal to that of the window, both periodic sinc() functions will present the same amount of aliasing, keeping the error controlled to some extent. We do not pretend that this technique provides the minimum error in every case, because one of the two sinc() functions can be more important than the other in some region. Especially because the visible margin of each sinc() function in the radiation pattern depends on the spacing between samples. This criterion is just a conservative approach to equilibrate the possible errors in a wide variety of cases.

Finally the number of sub-apertures employed in the window model must be specified. The far-field condition must be satisfied. In fact it will be better satisfied as the number of sub-apertures increases and as a result, the size of each one of them decreases. However, an increase in the number of sub-apertures requires a better description of the illumination near the window frame. The smaller the sub-aperture size, the worse the global uniform illumination approximation, since the sub-apertures on the center and the sub-apertures on the perimeter should not have the same illumination. So we choose to keep the size of the sub-apertures as big as possible without violating the far-field condition. As a result, the level of detail of the window description is kept as vague as possible. However this is compatible with an accurate statistical characterization of the fields, as we show in this paper.

2.2. Wall Modeling by Means of Image Theory

The presence of walls has an important influence on the field distribution inside the room. Although real windows are the main source of power density, walls behavior can be modeled by electric images of the main sources that take into account reflection in the walls. In summary we substitute the effect of the walls by the effect of these equivalent sources. Therefore, the final solution is just the superposition of the field radiated by the real apertures and their electric images. This approach simplifies the numerical solution because wall influence is treated using essentially the same tools that those needed to solve the real apertures.

In our work we assume that all the boundary surfaces are made of perfect electric conductor (PEC). However, more complex walls such as [28] are relatively easy to implement. In addition, we make no distinction between walls, ceiling, and floor. All of them are assumed to be PEC surfaces. That means that we do not take into account propagation through the exterior wall apart from that which

passes through the window panes. Similarly, we do not consider propagation through the closed door of the room neither through any other bounding surface. In summary, our proposed model is aimed to describe field variability and not the mean value of the field distribution, since relative rather than absolute values are sought.

Assuming a room with cuboid shape and only one exterior wall with two windows, Fig. 1 shows the real windows on the center together with images due to lateral walls, ceiling and floor. The diagonal of this matrix of images represents contributions that have been reflected in two orthogonal planes, for example wall-floor or wall-ceiling. The images in the center column or row, model reflections in two parallel planes: floor-ceiling or lateral walls. All the other elements in the matrix represent the rest of hybrid cases. With a similar reasoning, we could represent the images due to the other wall, opposite to the exterior wall.

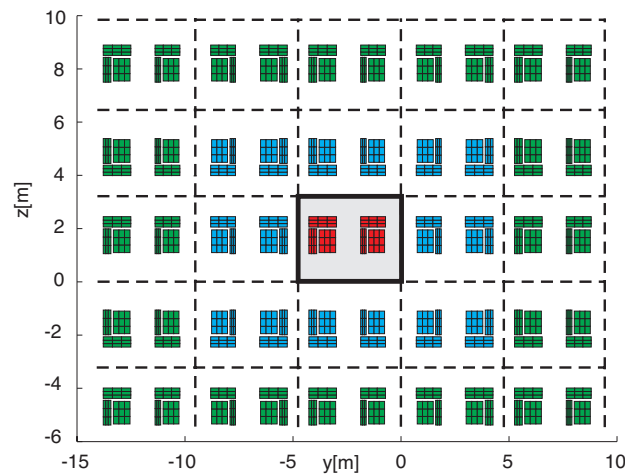


Figure 1. There are two real windows in the center. All the other windows are images of these ones. They take into account bounces on lateral walls, ceiling and floor. Each window pane is divided into 9 sub-apertures.

The classical theory of images is easy to apply to our problem. The position and orientation of the electric images depend on the relative position between the real aperture and each reflecting surface. For example, as we show in Fig. 2, the lateral electric image of a rotated window is similar to an image of the real window in a mirror placed on the wall. Accordingly, rotation about the horizontal axis of symmetry (see angle θ_r in Fig. 3) is replicated while a rotation about the vertical

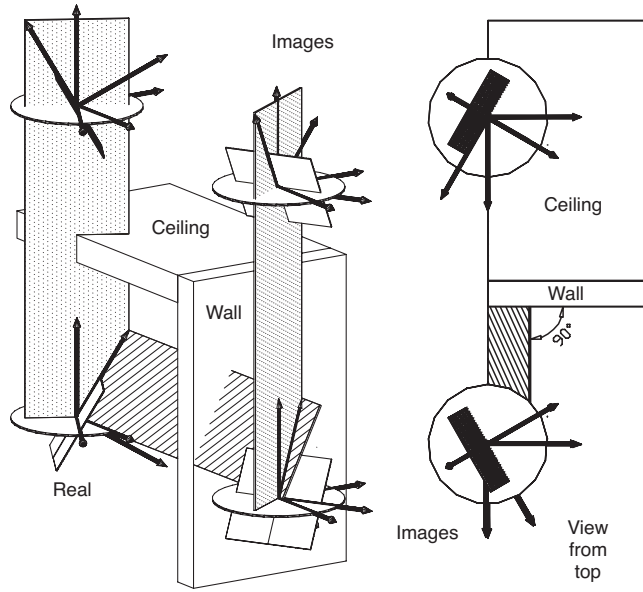


Figure 2. Images and boundary conditions. The only real aperture is on bottom left corner, all the other ones are images. The two on the right need a phase shift $\Delta\Phi_{PEC} = \pi$ to satisfy the boundary conditions since we employ vertical polarization in the apertures.

axis (angle ϕ_r) is changed in direction. Each rectangular cell in Fig. 1 contains two windows with three panes per window. Each sub-aperture inside the same rectangular cell has its own pair (ϕ_r, θ_r) so the incident wave front is not necessarily plane globally. However a sub-aperture and its images share the same pair $(|\phi_r|, |\theta_r|)$. Each element of the following matrices corresponds to the angle of rotation applied to one sub-aperture and its images. Each of them belongs to the rectangular cell of the i -th row and j -th column of Fig. 1:

$$(\phi_{r_{i,j}})_{5 \times 5} = \begin{pmatrix} \phi_r & -\phi_r & \phi_r & -\phi_r & \phi_r \\ \phi_r & -\phi_r & \phi_r & -\phi_r & \phi_r \\ \phi_r & -\phi_r & \phi_r & -\phi_r & \phi_r \\ \phi_r & -\phi_r & \phi_r & -\phi_r & \phi_r \\ \phi_r & -\phi_r & \phi_r & -\phi_r & \phi_r \end{pmatrix} \quad (2)$$

$$(\theta_{r_{i,j}})_{5 \times 5} = \begin{pmatrix} \theta_r & \theta_r & \theta_r & \theta_r & \theta_r \\ -\theta_r & -\theta_r & -\theta_r & -\theta_r & -\theta_r \\ \theta_r & \theta_r & \theta_r & \theta_r & \theta_r \\ -\theta_r & -\theta_r & -\theta_r & -\theta_r & -\theta_r \\ \theta_r & \theta_r & \theta_r & \theta_r & \theta_r \end{pmatrix} \quad (3)$$

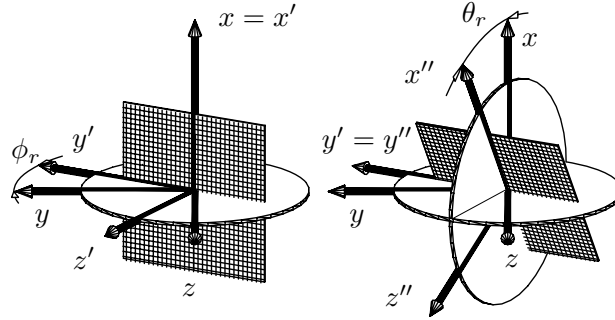


Figure 3. Rotation angles (ϕ_r, θ_r) . The hatched rectangles represent the sub-aperture. A generic rotation can be decomposed into two rotations. On the left we show the rotation around the vertical axis ($x = x'$). On the right we perform the rotation around the horizontal axis ($y' = y''$). The circles illustrate the planes of rotation.

The algorithm that finds the images is recursive. The final number of images depends on the number of consecutive reflections that we wish to take into account. Ray tracing algorithms usually allow two consecutive bounces.

Our sub-aperture E-fields will have vertical polarization in order to compare our model with previous results. Therefore, we apply a $\Delta\Phi_{PEC}$ phase shift to the lateral images in order to satisfy the boundary conditions for the E-field on the PEC walls. This means that images that are located in alternate columns have a relative phase difference of $\Delta\Phi_{PEC} = \pi$. For instance, in Fig. 1, all the sub-apertures inside the same rectangular cell have the same $\Delta\Phi_{PEC}$ correction. Each element $\Delta\Phi_{PEC_{i,j}}$ of the following matrix corresponds to the phase correction applied to the rectangular cell of the i -th row and j -th column of Fig. 1:

$$\left(\Delta\Phi_{PEC_{i,j}}\right)_{5 \times 5} = \begin{pmatrix} 0 & \pi & 0 & \pi & 0 \\ 0 & \pi & 0 & \pi & 0 \\ 0 & \pi & 0 & \pi & 0 \\ 0 & \pi & 0 & \pi & 0 \\ 0 & \pi & 0 & \pi & 0 \end{pmatrix} \quad (4)$$

2.3. Effective Area and Incidence Angle

The overall field emitted by the window sub-apertures must reconstruct the phase front that would be radiated from the whole window. In general, this phase front will not be parallel to the window plane, since

the emitter will not necessarily be in the direction perpendicular to the window plane as it is shown in Fig. 4. Accordingly, each sub-aperture is turned around its own geometrical center in order to assure that they all are locally parallel to the phase front of the incident wave. In addition, there will be a phase difference between them because each sub-aperture will not be reached at the same time by the incident phase front, as it is explained by the theory of arrays.

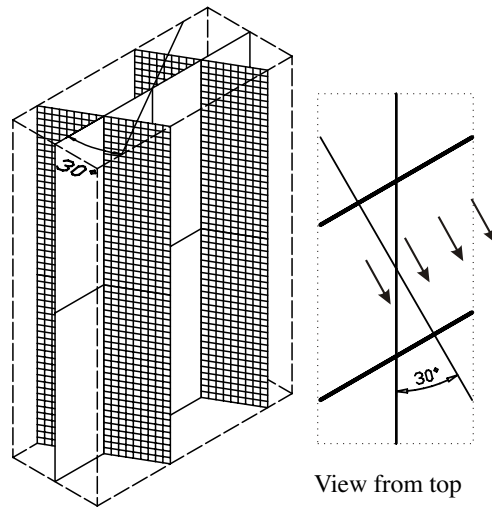
As stated before, the rotation angle is calculated separately for each sub-aperture. We use the straight lines that join the geometrical centers of the sub-apertures and the phase center of the exterior source of radiation to obtain each rotation angle. Therefore, the incident wave front is not necessarily plane globally. This is specially important if the exterior source is not very far away from the window. With respect to the phase difference between sub-apertures, we also use the same lines to get the path length differences between the several sub-aperture phase centers without any approximation. In this way it is not necessary that one of these lines becomes the reference to identify the plane wave direction and phase. A plane wave approach, with less computational load, is equivalent when the exterior emitter is far away from the window.

There is also another important issue related to the sub-aperture rotation, namely the effective area correction. As it is suggested in Fig. 4, if the sub-aperture size is not modified after performing the rotation, the sub-apertures will overlap when they are seen from the point of view of an observer placed on the emitter phase center. For example, in Fig. 4, we can see that the sub-aperture area must be reduced by 50% with an angle of incidence of 60° . If the angle of incidence is 90° the sub-aperture would collapse to a line segment. Till now, we have not characterized the model in this limit case. Therefore, we will restrict our discussion to smaller angles of incidence which in fact provide more power density inside the room. The size of each sub-aperture does not only affect to its radiated field intensity, but also to its radiation pattern. This fact is crucial to improve the accuracy of the calculations and will be addressed later.

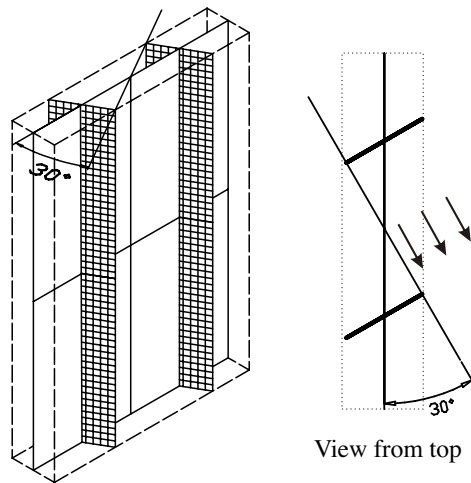
In order to evaluate the change in the sub-aperture effective size, we will decompose a general rotation into two simpler rotations, one around the x -axis (ϕ_r angle) and other one around the y -axis (θ_r angle). Both rotations are described in detail in Fig. 3. The effective area A_e could be calculated as:

$$A_e = h_e w_e = h \cos(\theta_r) w \cos(\phi_r) \quad |\phi_r| < \frac{\pi}{2}, |\theta_r| < \frac{\pi}{2} \quad (5)$$

where h_e and w_e are the sub-aperture effective height and width while h and w are respectively the height and width of the sub-aperture



(a) With overlapping error



(b) Without overlapping error

Figure 4. The white rectangles represent the sub-apertures before being rotated. The hatched ones show the same sub-apertures after being rotated. In Fig. 4(a) there is no sub-aperture resize, this fact leads to an overlapping error. In Fig. 4(b) this error is corrected by resizing the sub-apertures.

before the rotation.

In general, as we have just stated, sub-apertures will have two associated rotation angles (θ_r , ϕ_r) and we must rotate the radiation pattern of the sub-aperture consequently. This can be done by applying a rotation matrix to the Cartesian coordinates of the observation point in the local coordinate system (x , y , z) of the sub-aperture. This rotation allows to calculate the point coordinates in a new equivalent coordinate system (x'' , y'' , z''), obtained after rotating the initial one, as shown in Fig. 3. After that, we use the spherical coordinates (r'' , θ'' , ϕ'') of this rotated observation point to evaluate the following expression:

$$E_1 = \frac{E_0}{2\lambda r''} (1 + \cos \theta'') A_e \frac{\sin\left(\frac{k_x h_e}{2}\right)}{\frac{k_x h_e}{2}} \frac{\sin\left(\frac{k_y w_e}{2}\right)}{\frac{k_y w_e}{2}} \quad (6)$$

where the real constant E_0 is a scale factor which is applied to all the sub-apertures. It depends on the absolute power level of the transmitter. In addition, $k_x = \vec{\mathbf{k}} \cdot \hat{\mathbf{x}}''$ and $k_y = \vec{\mathbf{k}} \cdot \hat{\mathbf{y}}''$ are the Cartesian components of the vectorial wavenumber $\vec{\mathbf{k}} = k\hat{\mathbf{r}}''$. Finally, E-field components are obtained by substituting Eqn. (6) into:

$$E_{\theta''} = E_1 \cos(\phi'') e^{j(0.5\pi + \Phi_{PEC} - \Phi_{src} - kr'')} \quad (7)$$

$$E_{\phi''} = -E_1 \sin(\phi'') e^{j(0.5\pi + \Phi_{PEC} - \Phi_{src} - kr'')} \quad (8)$$

where Φ_{PEC} was defined in (4) and $\Phi_{src} = kd$ is the phase shift due to the distance d between the geometrical center of the sub-aperture and the phase center of the transmitting antenna.

The E-field emitted by the different sub-apertures must be obtained in a form that allows the application of the superposition principle. The overall process to achieve this result could be summarized as follows. Each observation point has absolute Cartesian coordinates in the room (x , y , z). To solve the electric field on the observation point due to one of the sub-apertures, the first step is to move the origin of coordinates to the center of the sub-aperture, (x , y , z) in Fig. 3. The second step would be to deal with the sub-aperture rotation by resizing it and obtaining the observation point coordinates in the rotated coordinate system (x'' , y'' , z''). Then we would convert the observation point from Cartesian to spherical coordinates. After that, we would employ the far field expression for the fields radiated by the sub-aperture taking into account its new effective area. Finally the resulting E-field vector must be expressed in Cartesian components in the (x , y , z) coordinate system in order to make it suitable for applying

the superposition principle with the E-field provided by the rest of sub-apertures in the same observation point. The Cartesian unitary vectors are invariant under translation.

The basic unit of our model is the sub-aperture, and the final solution is just the superposition of the influence of each of these sub-apertures on the observation points. As a result, this algorithm can be parallelized and it admits a simple workload management system because each observation point requires exactly the same computations that any other one. Consistently this algorithm has shown good parallelization scalability. The observation plane consists of a two-dimensional array of observation points. In our case an Open MP pragma parallelizes the for-loop whose index corresponds to the different segments of the observation plane. Also, we could share out the total number of sub-apertures between different cores instead of sharing out the observation points. However, the recursive nature of the classical electric image theory that is included in the algorithm makes this approach somewhat more complex without any additional advantage.

3. EXPERIMENTAL SETUP

The place selected to perform the experiment was an empty room on the second floor of our Faculty. As can be observed in the joint floor plan annexed (Fig. 5), roughly it is a rectangular-shaped room with two aluminum framed windows placed on the exterior wall and a wooden door on the opposite wall. The room has brick walls, false ceiling and tile floor. There are two pillars in the exterior wall corners. Exterior wall windows are shown in detail in Fig. 6, each window has three panes but the higher one is not included in the casement. The door and the windows remained closed during the experiment.

The transmitter was placed in another room of the second floor of the Faculty which is almost in front of the room under test. This is possible because our Faculty is an E-shaped building. We employed a Log-Periodic Dipole Antenna with vertical polarization to identify the direction from which the incident wave would be coming. The coordinates of the emitter in the axis shown in the upper right corner of Fig. 5 were $x = 1.78\text{m}$, $y = -11.35\text{m}$, $z = -23.5\text{m}$. Measurements were made at 900 MHz and a synthesized transceiver was used as transmitter.

The receiving antenna was a triaxial isotropic probe which was carried on a rail-guided vehicle. The special arrangement of the rails allowed this vehicle to cover a bidimensional surface in automatic mode [29]. The vehicle is driven by a motor controlled in turn by a laptop

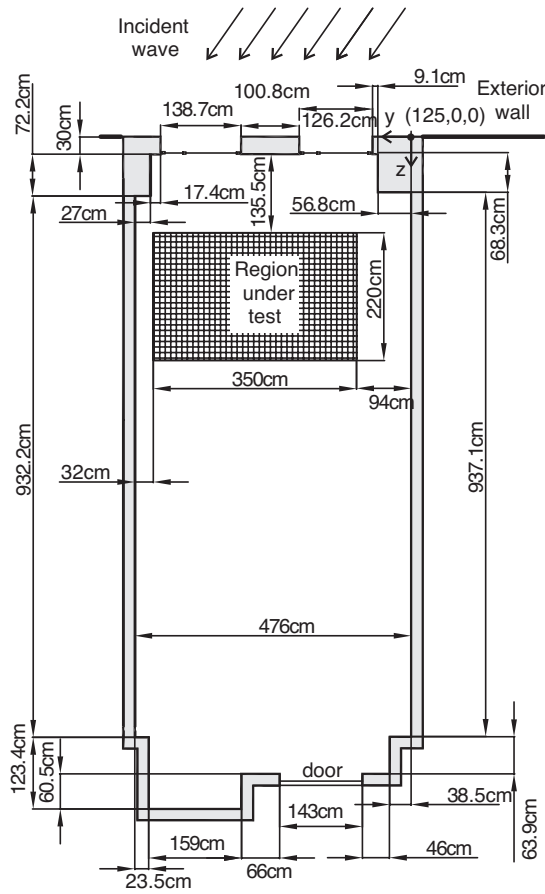


Figure 5. Floor plan. The region under test is at a height of 125 cm from the floor.

capable of synchronizing the movement with the measurement process carried out by means of a spectrum analyzer. The region under test was at 1.25 m height and the rectangular-shaped sampling grid cell had dimensions $2\text{ cm} \times 2\text{ cm}$. The whole region under test consists of a plain mesh with 175×110 sampling points, that is to say $n = 19,250$ measurement points in total. As the data sampling interval is less than a tenth of a wavelength, statistics deduced from measurements are identified as original ones. The measurement campaign was carried out during two weeks but in spite of the interruptions, as expected, due to the stationary nature of the field distribution inside the room, this lack of continuity becomes irrelevant. The measurement period was

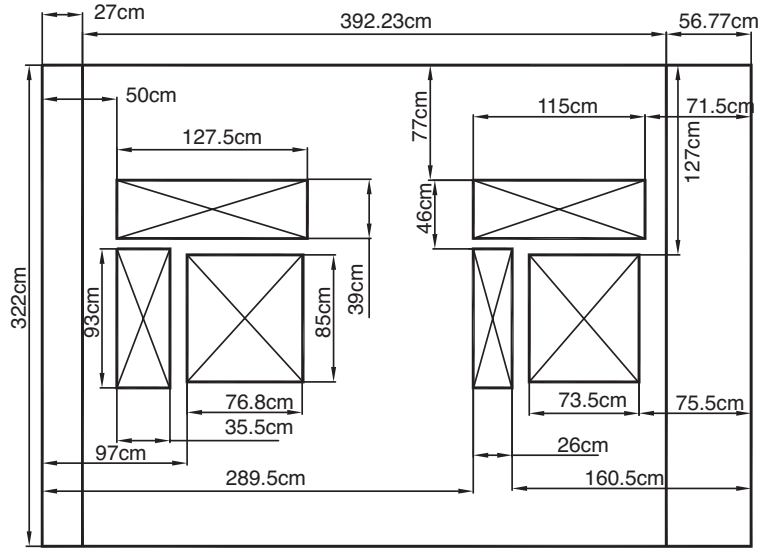


Figure 6. Exterior wall. Interior elevations.

characterised by relatively dry and stable weather conditions [30].

The aim of our model is not to predict the field envelope on a point-by-point basis, since the necessary level of detail of the input data would make the data collection process impractical. Therefore, instead of taking into account the pillars and the overall irregular shape of the floor plan, we have adopted the cuboid that fits better inside the empty volume of the room. In particular, our room model is a cuboid with $\Delta z = 11.7$ m, $\Delta y = 4.76$ m and $\Delta x = 3.22$ m. Note that we place the apertures on the exterior surface of the windows wall. The windowsill and the wall thickness are eliminated. In addition we do not consider the materials which compose the walls, ceiling, floor and door. All the room surfaces except window panes are substituted by perfect electric conductor.

4. SUB-APERTURE MODEL RESULTS

Our final purpose is to get an estimation of the electric field envelope Cumulative Distribution Function (CDF) of the vertical electric field in the region under test by means of the simulation of the simplified model. In order to quantify the goodness of fit of our approximation we employ the Kolmogorov-Smirnov (KS) test to study whether the two underlying one-dimensional probability distributions differ. In our

Table 1. The goodness of fit: P-values.

H/V	1	2	3	4	5
1	0.1336	0.1784	0.2621	0.2472	0.2468
2	0.5290	0.2423	0.1837	0.1755	0.1768
3	0.7002	0.9608	0.9895	0.9913	0.9925
4	0.1031	0.1472	0.1204	0.1314	0.1410
5	0.3919	0.6593	0.4000	0.4017	0.3971

case, the KS statistic $D_{n,n'}$ will be:

$$D_{n,n'} = \sup_x |F_n(x) - F_{n'}(x)| \quad (9)$$

where $F_n(x)$ and $F_{n'}(x)$ are the empirical CDFs obtained from the real measurements and from the simulation respectively, given that $n = 19,200$ is the number of measurement points in the real sampling grid, as we stated before, and $n' = 6,930$ is the number of points in the simulation sampling grid ($0.1\lambda \times 0.1\lambda$). The null hypothesis is that both sets of samples come from the same distribution and the P-value P_{KS} gives the probability that one would actually observe such a $D_{n,n'}$ given that the null hypothesis is true. In particular, the P-value is obtained approximately from [31]:

$$P_{KS} = 1 - F_K \left(D_{n,n'} \left[\sqrt{N_e} + 0.12 + \frac{0.11}{\sqrt{N_e}} \right] \right) \quad (10)$$

where $N_e = \frac{nn'}{n+n'}$ is the effective number of data points and F_K is the Kolmogorov CDF given as:

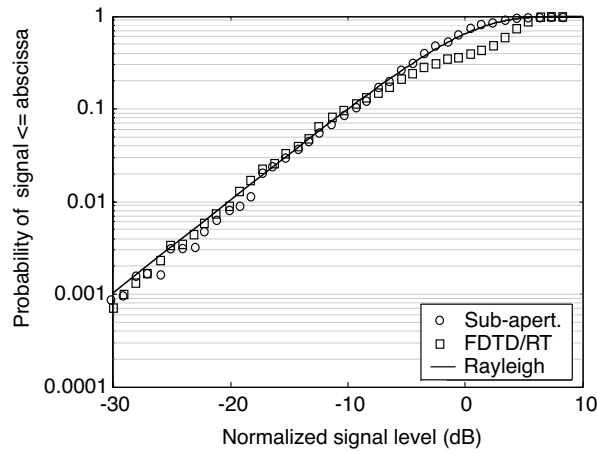
$$F_K(\lambda) = 1 - 2 \sum_{j=1}^{\infty} (-1)^{j-1} e^{-2j^2\lambda^2} \quad (11)$$

The goodness of fit of the proposed method to the experimental data is summarized in Tab. 1, where H and V are the number of sub-apertures in the horizontal and vertical direction employed for each simulation. As was stated before ($H = 3$, $V = 3$), shown in Fig. 1, provides one of the best results.

We have also included $D_{n,n'}$ values in Tab. 2. They show the maximum deviation between the measured and simulated experimental CDFs.

Table 2. Maximum distance between measured and simulated CDFs.

H/V	1	2	3	4	5
1	0.0163	0.0154	0.0141	0.0143	0.0143
2	0.0113	0.0144	0.0153	0.0154	0.0154
3	0.0099	0.0071	0.0062	0.0061	0.0060
4	0.0170	0.0160	0.0166	0.0163	0.0161
5	0.0126	0.0102	0.0125	0.0125	0.0125

**Figure 7.** The proposed method clearly outperforms FDTD/RT at fitting E-field envelope experimental CDF.

5. DISCUSSION

An important issue is how robust the proposed method is to errors in the transmitter position determination. To address this issue we present Fig. 8. It shows a P-value ($H = 3$, $V = 3$) for each point on the surface of the window where the transmitter antenna was placed, as if the center of phase of the antenna is precisely on that point. In our experiment, the transmitter antenna was placed on the zone with higher P-values, but if there is an error in the phase center location, the P-values remain high in the neighboring points so the model is equally useful.

In order to compare the proposed method with previous models, we have taken as reference [32], an experimental work which was employed in [4] and [18] to show how Ray-Tracing and FDTD/RT

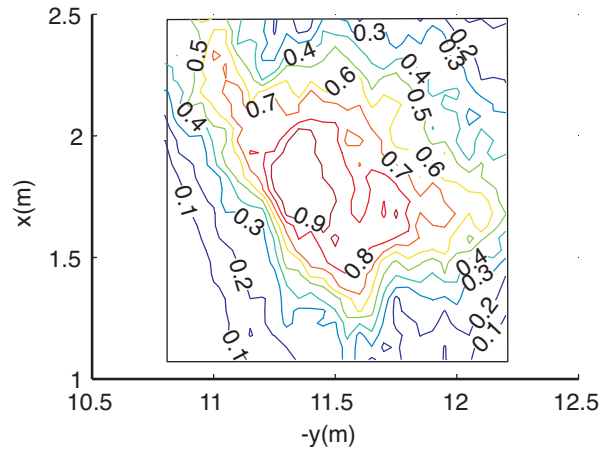


Figure 8. P-value obtained assuming that the center of phase of the transmitter is situated in different points of the window through which the source signal was going out.

perform in the outdoor/indoor propagation problem. In particular, [18] explained how a hybrid method outperforms a pure ray-tracing method for this type of problem. In fact, ray tracing fails to follow the fast-fading variations while the hybrid method yields a much better approximation to the experimental distribution found in [32]. In turn, we want to state that our method clearly improves the results obtained by [18].

The experimental setup used by [32] is quite similar to the one employed in our work. A scanning device measured the vertical component of the E-field (1290 MHz) inside a room radiated by an exterior antenna with vertical polarization. In summary, this measurement campaign provided approximately a Rayleigh distribution and therefore [18] compares its simulation results with this distribution. In Fig. 7 we compare our results with those obtained by [18]. Their sample space was a segment parallel to the exterior wall. More exactly, this segment was placed 5λ away from the windows. As can be seen, FDTD/RT gets a maximum deviation around $D_{n,n'} = 30\%$, which would mean a P-value of $2.4e-52$. Our fit is much more accurate. It is not possible to read the maximum deviation of our method in that plot with precision. As an alternative, we have found the Rayleigh that better fits our data and we have found a maximum deviation of $D_{n,n'} = 3.35\%$ employing 645 samples (0.1λ spacing, $N_e = 645$ in Eqn. (10)). This maximum deviation corresponds to a P-value of 0.46, several orders of magnitude better than the one

obtained with FDTD/RT. However, it must be noted that the KS test is not accurate if the CDF is estimated from the simulated data (it could be too optimistic). But we have to take into account that we work in both cases with the same rules. Previous works did not apply the KS test to test the goodness of fit and therefore they did not have to worry about this issue.

6. CONCLUSIONS

The model presented here provides a basis to quantitatively predict and analyze the field distribution obtained in outdoor/indoor propagation through window structures with a high degree of accuracy in comparison to previous methods. It makes it easy to deal with 3 dimensions and includes parallel processing in a straightforward and practical way to speed calculations. In fact, it outperforms FDTD and RT based methods in speed and accuracy, reducing the amount of detail needed to initialize the model at the same time. The goodness of fit test provides P-values around 99%, or equivalently a maximum error between the measured and simulated CDFs of less than 0.7% taking into account several thousands of samples.

ACKNOWLEDGMENT

This work was supported in part by the Regional Ministry for Public Works of the Junta de Castilla y León.

REFERENCES

1. Iskander, M. F. and Z. Yun, "Propagation prediction models for wireless communication systems," *Transactions on Microwave Theory and Techniques*, Vol. 50, 662–673, 2002.
2. Seidel, S. Y. and T. S. Rappaport, "Site-specific propagation prediction for wireless in-building personal communication system design," *IEEE Transactions on Vehicular Technology*, Vol. 43, 879–891, 1994.
3. Corazza, G. E., V. Degli-Esposti, M. Frullone, and G. Riva, "A characterization of indoor space and frequency diversity by ray-tracing modeling," *IEEE Journal on Selected Areas in Communications*, Vol. 14, 411–419, 1996.
4. Yang, C., B. Wu, and C. Ko, "A ray-tracing method for modeling indoor wave propagation and penetration," *IEEE Transactions on Antennas and Propagation*, Vol. 46, 907–919, 1998.

5. Liang, G. and H. L. Bertoni, "A new approach to 3D ray tracing for propagation in cities," *IEEE Transactions on Antennas and Propagation*, Vol. 46, 853–863, 1998.
6. Zhang, Z., K. R. Soresen, Z. Yun, M. F. Iskander, and J. F. Harvey, "A ray-tracing approach for indoor/outdoor propagation through window structures," *IEEE Transactions on Antennas and Propagation*, Vol. 50, 742–748, 2002.
7. Kara, A. and E. Yazgan, "Modelling of shadowing loss due to huge non-polygonal structures in urban radio propagation," *Progress In Electromagnetics Research B*, Vol. 6, 123–134, 2008.
8. Wang, N., Y. Zhang, and C. H. Liang, "Creeping ray-tracing algorithm of UTD method based on NURBS models with the source on surface," *Journal of Electromagnetics Waves and Applications*, Vol. 20, No. 14, 1981–1990, 2006.
9. Liang, C., Z. Liu, and H. Di, "Study on the blockage of electromagnetic rays analytically," *Progress In Electromagnetics Research B*, Vol. 1, 253–268, 2008.
10. Blas, J., F. A. Lago, P. Fernández, R. M. Lorenzo, and E. J. Abril, "Potential exposure assessment errors associated with body-worn RF dosimeters," *Bioelectromagnetics*, Vol 28, 573–576, 2007.
11. Wang, M. Y., J. Xu, J. Wu, Y. B. Yan, and H. L. Li, "FDTD study on scattering of metallic column covered by double-negative metamaterial," *Journal of Electromagnetic Waves and Applications*, Vol. 21, No. 14, 1905–1914, 2007.
12. Lee, F. W. H. and A. K. Y. Lai, "FDTD analysis of indoor radio propagation," *IEEE International Symposium on Antennas and Propagation Society*, Vol. 13, 1664–1667, 1998.
13. Pahlavan, K. and A. H. Levesque, *Wireless Information Networks*, Wiley Series in Telecommunications and Signal Processing, Wiley, 1995.
14. Talbi, L. and G. Y. Delisle, "Finite difference time domain characterization of indoor radio propagation," *Progress In Electromagnetics Research*, PIER 12, 251–275, 1996.
15. Ali, M. and S. Sanyal, "A numerical investigation of finite ground planes and reflector effects on monopole antenna factor," *Journal of Electromagnetic Waves and Applications*, Vol. 21, No. 10, 1379–1392, 2007.
16. Uduwawala, D., "Modeling and investigation of planar parabolic dipoles for GPR applications: A comparison with bow-tie using FDTD," *Journal of Electromagnetic Waves and Applications*, Vol. 20, No. 2, 227–236, 2006.

17. Golestani-Rad, L., J. Rashed-Mohassel, and M. M. Danaie, "Rigorous analysis of EM-wave penetration into a typical room using FDTD method: The Transfer Function concept," *Journal of Electromagnetic Waves and Applications*, Vol. 20, No. 7, 913–926, 2006.
18. Wang, Y., S. Safavi-Naeini, and S. K. Chaundhuri, "A hybrid technique based on combining ray tracing and FDTD methods for site-specific modeling of indoor radio wave propagation," *IEEE Transactions on Antennas and Propagation*, Vol. 48, 743–754, 2000.
19. Bernardi, P., M. Cavagnaro, S. Pisa, and E. Piuze, "Human exposure to radio base-station antennas in urban environment," *IEEE Transactions on Microwave Theory and Techniques*, Vol. 48, 1996–2002, 2000.
20. Bernardi, P., M. Cavagnaro, P. D'Atanasio, E. Di Palma, S. Pisa, and E. Piuze, "FDTD, multiple-region/FDTD, ray-tracing/FDTD," *International Journal of Numerical Modelling*, Vol. 15, 579–593, 2002.
21. Bernardi, P., M. Cavagnaro, R. Ceccetti, S. Pisa, E. Piuze, and O. Testa, "A UTD/FDTD investigation on procedures to assess compliance of cellular base-station antennas with human-exposure limits in a realistic urban environment," *Transactions on Microwave Theory and Techniques*, Vol. 51, 2109–2417, 2003.
22. Martínez-Búrdalo, M., A. Martín, V. Pizarro, and R. Villar, "An efficient FDTD-time-domain equivalent currents method for safety assessment in human exposure to base-station antennas in presence of obstacles," *Microwave and Optical Technology Letters*, Vol. 48, 1987–1990, 2006.
23. Simthson, A. G. and I. A. Glover, "Prediction of attenuation and delay-spread for systems with outdoor basestations and indoor users," *Proceedings of the 9th European Conference on Wireless Technology*, 265–268, 2006.
24. Noori, N. and H. Oraizi, "Evaluation of MIMO channel capacity in indoor environments using vector parabolic equation method," *Progress In Electromagnetics Research B*, Vol. 4, 13–25, 2008.
25. Guo, S. X., Y. Gao, and L. X. Zhang, "Simulation research on turbo equalization algorithm based on microwave fading channel," *Progress In Electromagnetics Research Letters*, Vol. 4, 99–107, 2008.
26. Wu, B. I., F. C. A. I. Cox, and J. A. Kong, "Experimental methodology for non-thermal effects of electromagnetic radiation on biologics," *Journal of Electromagnetic Waves and Applications*,

- Vol. 21, No. 4, 533–548, 2007.
27. Lee, S. H. and R. C. Rudduck, “Aperture integration and GTD techniques used in the NEC reflector antenna code,” *IEEE Transactions on Antennas and Propagation*, Vol. 33, 189–194, 1985.
 28. Teh, C. H., F. Kung, and H. T. Chuah, “A path-corrected wall model for ray-tracing propagation modeling,” *Journal of Electromagnetic Waves and Applications*, Vol. 20, No. 2, 207–214, 2006.
 29. Blas, J., A. Bahillo, S. Mazuelas, D. Bullido, P. Fernández, R. M. Lorenzo, and E. J. Abril, “Scanning device for sampling the spatial distribution of the E-field,” *Proceedings of World Academy of Science, Engineering and Technology*, Vol. 14, 199–203, 2007.
 30. Helhel, S., Ş. Özen, and H. Göksu, “Investigation of GSM signal variation depending weather conditions,” *Progress In Electromagnetics Research B*, Vol. 1, 147–157, 2008.
 31. Press, W. H., B. P. Flannery, S. A. Teukolsky, and W. T. Vetterling, *Numerical Recipes in C: The Art of Scientific Computing*, 2nd edition, Cambridge University Press, Cambridge, England, 1992.
 32. Horikoshi, J., D. Tanaka, and T. Morinaga, “1.2 GHz band wave propagation measurements in concrete building for indoor radio communications,” *IEEE Transactions on Vehicular Technology*, Vol. 35, 146–152, 1986.